Chronic septal infarction confers right ventricular protection during mechanical left ventricular unloading

James Mau, BSc, MB, BS,[a] Stuart Menzie, MB, BS, FRACS,[a] Yifei Huang, MD, PhD,[a] Michael Ward, MB, BS, PhD, FRACP,[b] and Stephen Hunyor, MB, BS, MD, MTM, FRACP, FACC[a,b]

Objective: Right ventricular failure manifests in 25% of left ventricular assist device recipients because of ventricular coupling mechanism disruption. Septal ischemia accentuates this process, but the effect of septal infarction has not been elucidated. Right ventricular response to incremental left ventricular unloading was studied in sheep with septal infarction.

Methods: Septal infarction was induced in 6 sheep using ethanol delivery into the main septal perforating artery. Six shams avoided ethanol. Load-independent and in-series right ventricular response to incremental (0%–100%) left ventricular unloading was measured 4 weeks later. Dimensions of whole heart, wall thickness, and chamber volumes were obtained using sonomicrometers. Selective perfusion with triphenyltetrazolium quantified septal damage.

Results: Right ventricular preload-recruitable-stroke-work, contractility, and ejection fraction were lower at 75% and 100% left ventricular unloading in sham compared with infarcted animals (75%: 26.3 ± 3.4, 0.70 ± 0.15, and 23.9 ± 4.6 vs 37 ± 2.6 erg*10^3, 0.99 ± 0.18 mm Hg/mL, and 35.5% ± 3.4%, all $P < .01$, 100%: 24.8 ± 4.5, 0.67 ± 0.14, and 23.8 ± 5.8 vs 36.0 ± 4.6 erg*10^3, 0.90 ± 0.09 mm Hg/mL, and 32.7% ± 11.0%, all $P < .01$). Central venous pressure was higher at 75% and 100% unloading in sham compared with infarcted animals (75%: 8.6 ± 1.0 vs 4.5 ± 1.0, 100%: 12.4 ± 0.8 vs 3.4 ± 1.0 mm Hg, all $P < .01$). Right ventricular cardiac output was less in shams with 100% unloading (1.2 ± 0.2 L/min vs 2.1 ± 0.3 L/min, $P < .01$). End-diastolic and end-systolic right ventricular short-axis dimension at 75% and 100% unloading was greater in sham compared with infarcted animals (75%: 34.4 ± 5.5 mm and 29.1 ± 5.5 mm vs 25.6 ± 4.7 mm and 20.5 ± 4.0 mm; 100%: 37.6 ± 6.6 mm and 29.9 ± 5.9 mm vs 25.5 ± 3.9 mm and 21.1 ± 3.8 mm, all $P < .01$). Prolonged diastolic relaxation (Tau) in infarcted animals was normalized with 75% and 100% unloading.

Conclusion: High-level (≥75%) left ventricular unloading causes right ventricular dilatation and compromised function. Chronic septal damage, however, confers protection by preserving right ventricular dimensions.

ET/BS

Implantation of left ventricular assist devices (LVADs) for the treatment of heart failure has increased in the post REMATCH era,[1] with several devices now approved as destination therapy.[2,3] However, LVAD placement is complicated by perioperative right ventricular (RV) failure in up to 25% of recipients.[4,5] This leads to inadequate LVAD filling and reduced cardiac output (CO), and if severe often necessitates placement of an additional device to support right-sided circulation,[5] with associated high risk and costs.[2] Prolonged inotrope use is often required, and elevated central venous pressure (CVP) leads to compromised multiple organ function.[6] Thus, prediction of RV failure susceptibility before commencement of LVAD support could minimize morbidity and mortality, and reduce operating room and intensive care costs. In the absence of coexisting heart pathology, LVAD use has been shown to independently alter RV contractility,[7] load,[8] and compliance.[9] The resulting effects on septal geometry lead to disruption of mechanisms that regulate ventricular interdependence[10-12] and affect RV pressures and volumes. Temporary septal ischemia during high-level left ventricular (LV) unloading has been shown to accentuate these changes.[13] However, the effects of irreversible septal damage with associated changes in septal tissue compliance and contractility remain to be elucidated. Refinement of septal ablation techniques[14] has prompted such a study in a large animal model. Resulting pathology resembles that seen clinically in humans after acute infarction of the septal perforating artery supply area.[15,16] We previously showed that acute and chronic RV hemodynamic responses are distinctly different after septal injury, the former suggestive of paradoxical motion and the latter

From the Cardiac Technology Centre, Kolling Institute,[a] St Leonards, Australia; and Department of Cardiology,[b] University of Sydney at Royal North Shore Hospital, Sydney, Australia.

This project was supported by the National Health and Medical Research Council of Australia (NHMRC; Grant 262031) and the North Shore Heart Research Foundation (Grants 16-04/05 and 19-01/02). James Mau is a Dora Lush Scholar of the NHMRC.

Received for publication Nov 7, 2008; revisions received Feb 19, 2009; accepted for publication March 9, 2009.

Address for reprints: James Mau, BSc, MB, BS, Cardiac Technology Centre, Kolling Bld, Royal North Shore Hospital, Pacific Hwy, St Leonards, Sydney, NSW, Australia 2065 (E-mail: jmau@med.usyd.edu.au).

J Thorac Cardiovasc Surg 2009;138:172-8
0022-5223/$36.00

doi:10.1016/j.jtcvs.2009.03.012

Abbreviations and Acronyms

CO = cardiac output
CVP = central venous pressure
ED = end diastolic
EF = ejection fraction
ES = end systolic
LV = left ventricular
LVAD = left ventricular assist device
PRSW = preload recruitable stroke work
PTSMA = percutaneous transluminal septal myocardial ablation
RV = right ventricular

suggestive of reduced compliance and buttress formation.[17] A chronic model of septal dysfunction using percutaneous transluminal septal myocardial ablation (PTSMA) was induced in sheep prior to mechanical LV unloading using a centrifugal device. Both load-independent[18] and in-series RV hemodynamic function were measured.

MATERIALS AND METHODS

Anesthesia

Eighteen Border Leicester cross sheep (body weight 61.7 ± 8.8 kg) were used in this study. The protocol was approved by the Institutional Animal Care and Ethics Committee, and animals received humane care in compliance with the ''Guide for the Care and Use of Laboratory Animals'' prepared by the Institute of Laboratory Animal Resources, National Research Council, 1996. Anesthesia was induced by alfaxalone (5–10 mg/kg, Alfaxan-CD RTU; Jurox Pty Ltd, Rutherford, Australia) and maintained with 50% oxygen, 45%/50% nitrous oxide, and approximately 2% isoflurane (Mayne-Pharma, Melbourne, Australia). Regular blood gas measurements were used to maintain physiologic ventilation and oxygenation.

Study Design

All animals were acclimatized for at least 2 weeks before randomization into 2 experimental arms involving selective percutaneous over-the-wire cardiac catheterization of the main septal perforating artery (MSPA) with either sham or active PTSMA. After a 4-week recovery period, RV hemodynamic and dimensional changes were measured in response to incremental LV unloading (0%–100% in 4 equal steps) using a Biomedicus centrifugal pump. Hemodynamic measurements followed at least 30 minutes of stable anesthesia and were taken at end expiration. After functional profiling, the heart was harvested for histologic analysis.

Baseline Ablative Procedure

Right and left jugular veins and the right carotid artery were cannulated, and a 53-cm bipolar pacemaker lead (Medtronic Capsure SP-4524; Medtronic, Minneapolis, Minn) was secured to the RV apex. A single-chamber pacemaker (Sigma Series SR 300; Medtronic) was set to activate at a hysteresis of 50 bpm and pace at 80 bpm as a rescue device for heart block. A 2.0 × 9-mm over-the-wire balloon catheter (Maverick SoftLEAP Boston Scientific, Natick, Mass) was mounted on a 0.014-inch hydrocoat guidewire (Hi Torque Guidant Balance Middleweight; Guidant Corporation, St Paul, Minn) and guided into the MSPA angiographically via the carotid artery before being positioned with proximal clearance of the left anterior descending. Correct positioning of the balloon markers within the MSPA with subsequent angiographically verified arterial patency was considered completion of a sham-ablative procedure. For septal ablation, the balloon was inflated to 8 ATM, and an immediate bolus volume of 0.6 mL 99.6% ethanol was delivered. Ten minutes after balloon deflation and removal, MSPA closure was verified angiographically. Pacemaker performance was checked 4 weeks later, immediately before terminal hemodynamic assessment.

Left Ventricular Unloading and Terminal Hemodynamic Assessment

Four weeks after septal ablation, Millar catheters were positioned in the LV and RV, and a 7F triple lumen Swan-Ganz catheter was positioned in the pulmonary circuit. The heart and great vessels were accessed through a left thoracotomy with removal of the fifth rib. Transonic flow probes (MA-16 and MA-20PAX; Transonic Systems Inc, Natick, NY) were placed around the ascending aorta and pulmonary trunk after incision of the pericardium from apex to its reflection. Ten sonomicrometer crystals (2 mm Silastic; Sonometrics Corp, Ontario, Canada) were attached in epicardial and endocardial positions (Figure 1). Before implantation, paired crystals underwent bench calibration in normal saline solution to verify signal strength and accuracy. The ascending aorta was cannulated at the division of the brachiocephalic trunk using a 20F reinforced pump head outflow cannula (Select Series 72220; Medtronic Inc) and secured with 2 snugged 4-0 Prolene purse string sutures. The left atrial appendage was isolated and cannulated using a 36F inflow cannulae (DLP-68136; Medtronic Inc) that traversed the mitral valve. The distal cannula tip was positioned approximately 25 mm above the LV apex. The cannulae were connected to a centrifugal hemopump (Biomedicus series 540/BP-80 pump head; Medtronic Inc), and tubing dead space was filled using 400 mL heparinized Hartman's solution. An automated coagulation timer (ACT-II; Medtronic Inc) monitored clotting status, with activated clotting time maintained using heparin at 230 to 250 seconds. Actual mechanical bypass values were matched with values from the pulmonary flow probe. All hemodynamic measurements were assessed at 4 incremental levels of LV unloading (0%, lines clamped, to 100%, as measured by pulmonary flow probe). Thirty minutes of stable unloading preceded all hemodynamic measurements, which included ejection fraction (EF), CVP, RV CO, Tau, Ees, and preload recruitable stroke work (PRSW). RV volume was derived from an ellipsoid subtraction model[19] with SV calibrated against pulmonary flow probe values.

Septal Geometric, Functional, and Histologic Assessment

Crystal positions, confirmed at autopsy to be in an equatorial plane across the cardiac short axis, measured RV and LV internal dimension and LV, RV free-wall, and septal thickness. Histologic analysis involved selective MSPA perfusion using 1% triphenyltetrazolium solution and simultaneous differential staining of the left main and right coronary arteries.

Data Analysis

End-diastolic (ED) and end-systolic (ES) dimensions were analyzed as described previously.[17] ED was defined as the time of peak electrocardiogram-R wave and LV and RV ES as the point of zero aortic or pulmonary flow, respectively. Steady-state hemodynamic parameters were calculated as the average of 8 to 10 beats. PRSW relationship was calculated from the plot of SW against loading end-diastolic volume and ESPVR slope as described previously.[20] Coded randomized digital photos were analyzed by a blinded operator using planimetry (Sigma Scan Image v2.03, SPSS Inc, Chicago, Ill).

Statistical Analysis

Results are reported as means or percentages ± standard deviation as appropriate. For all parameters, comparisons between groups were calculated using either a 2-tailed *t* test for parametric distributions or a Mann–Whitney rank-sum test for nonparametric distributions (SigmaStat Statistical Software v2.03; SPSS Inc, Chicago, Ill).

ET/BS

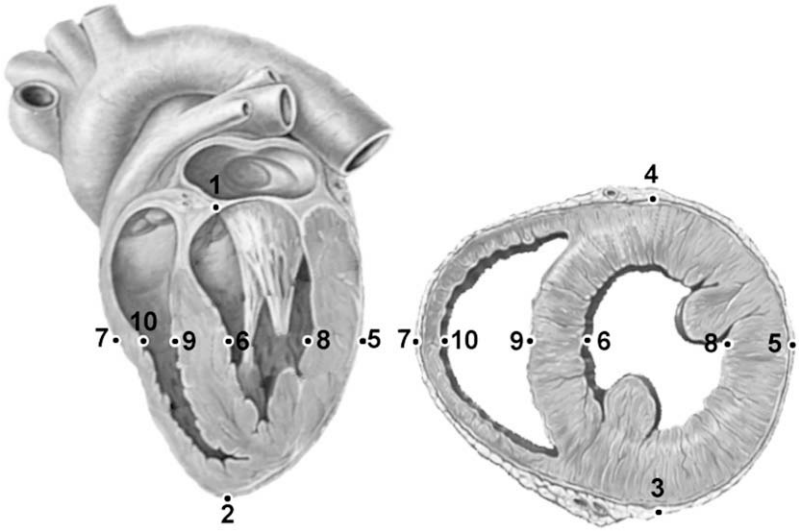

FIGURE 1. Cardiac long-axis and mid-papillary short axis sections showing implanted sonomicrometer crystal positions. Epicardial crystal placements: *1* and *2*, base and apex dimension; *3* and *4*, anterior and posterior midpapillary short axis dimension; *5* and *7*, LV plus RV lateral mid-papillary short axis dimension. Endocardial crystal placements: *6* and *9*, septal LV and RV mid-papillary surface; *8* and *10*, free wall LV and RV mid-papillary surface.

RESULTS

Six animals for both ablation and sham groups were used for analysis. Two animals died acutely of heart failure or irrecoverable arrhythmias after PTSMA, and 3 others died after placement of sonomicrometer crystals or LV unloading device. One animal was excluded because amiodarone had been used.

Load-Independent Systolic and Diastolic Function

Load-independent hemodynamic data in Figure 2 shows stable RV PRSW in PTSMA animals across all assist levels, averaging 47.8 ± 7.0 erg*10^3/mL. In sham animals, despite stability with 0%, 25%, and 50% unloading (averaging 48.1 ± 10.8 erg*10^3/mL), RV PRSW decreased to 35.0 ± 4.5 erg*10^3/mL, $P \leq .01$ with 75% unloading, and remained at this level with 100% unloading (33.0 ± 6.0 erg*10^3/mL, $P \leq .01$). Values with 75% or greater unloading were comparatively lower in the sham group (35.0 ± 4.5 and 33.0 ± 6.0 erg*10^3/mL vs 49.2 ± 3.5 and 47.9 ± 6.1 erg*10^3/mL, $P \leq .01$). RV Ees in PTSMA animals remained stable across all assist levels, averaging 0.93 ± 0.12 mm Hg/mL. In sham animals, it increased with 25% unloading (1.12 ± 0.15 mm Hg/mL vs 0.94 ± 0.13 mm Hg/mL; $P \leq .01$) but returned to baseline with 50% (0.88 ± 0.08 mm Hg/mL vs 0.92 ± 0.13 mm Hg/mL; $P = .472$) before decreasing to 0.70 ± 0.15 mm Hg/mL and 0.67 ± 0.14 mm Hg/mL with 75% and 100% unloading, respectively. Values at 75% or greater unloading were lower in sham animals (0.70 ± 0.15 mm Hg/mL and 0.67 ± 0.14 mm Hg/mL vs 0.99 ± 0.18 mm Hg/mL and 0.90 ± 0.09 mm Hg/mL, $P \leq .01$). Before device insertion and with 0% and 25% unloading, RV Tau was prolonged in PTSMA (no device: 28.0 ± 4.0 ms vs 22.8 ± 4.5 ms, 0%: 32.5 ± 4.8 ms vs 21.5 ± 2.0 ms, 25%: 27.5 ± 4.9 ms vs 26.0 ± 4.9 ms sham; $P \leq .01$); however, PTSMA induced prolongation normalized with 50%, 75%, and 100% unloading.

Load-Dependent Right Ventricular Function

RV EF (Figure 3) remained stable in PTSMA animals independently of LV unloading, averaging 34.8% ± 9.8%. In contrast, RV EF decreased in sham animals to 23.9% ± 4.6% with 75% and 100% unloading ($P \leq .01$) and was lower compared with equivalent PTSMA values (75%: 23.9% ± 4.6% vs 35.5% ± 3.4%, 100%: 23.8% ± 5.8% vs 32.7% ± 11.0%, all $P \leq .01$). CVP remained stable across all assist levels in PTSMA animals but increased in the sham group from 4.2 ± 1.7 mm Hg with 50% unloading to 8.6 ± 1.0 mm Hg with 75%, and to 12.4 ± 0.8 mm Hg with 100% unloading (all $P \leq .01$). Values with 75% or greater unloading were comparatively higher in sham compared with PTSMA (75%: 8.6 ± 1.0 mm Hg and 12.4 ± 0.8 mm Hg vs 4.5 ± 1.0 mm Hg, 100%: 3.4 ± 1.0 mm Hg PTSMA, all $P \leq .01$). RV CO was stable in PTSMA animals during all levels of unloading, averaging 2.1 ± 0.3 L/min. In sham animals, after being stable with 0% to 75% unloading averaging 2.3 ± 0.5 L/min, it dipped by approximately 50% with 100% unloading (1.2 ± 0.2 L/min vs 2.1 ± 0.3 L/min, $P \leq .01$).

Dimensional Changes

RV and LV internal short-axis dimensions are summarized in Table 1. There were no significant differences in either group between RV and LV ED and ES internal dimensions with 0%, 25%, and 50% LV unloading. However, respective RV dimensions increased from 27.8 ± 6.0 mm and 21.7 ± 5.9 mm with 50% unloading to 34.4 ± 5.5 mm and 29.1 ± 5.5 mm with 75% unloading ($P \leq .01$) and were significantly higher when compared with

ET/BS

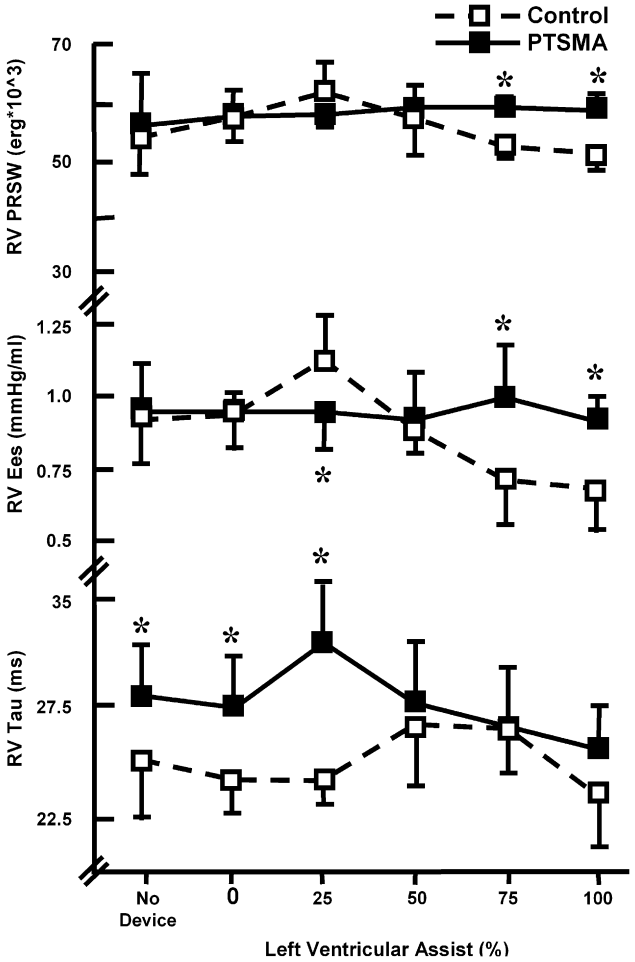

FIGURE 2. Load-independent hemodynamic effects of LV unloading in sham and PTSMA animals. *RV PRSW,* Right ventricular preload recruitable stroke work; *RV Ees,* right ventricular end-systolic elastance; *RV Tau,* time (ms) of RV diastolic relaxation constant; *PTSMA,* percutaneous transluminal septal myocardial ablation.

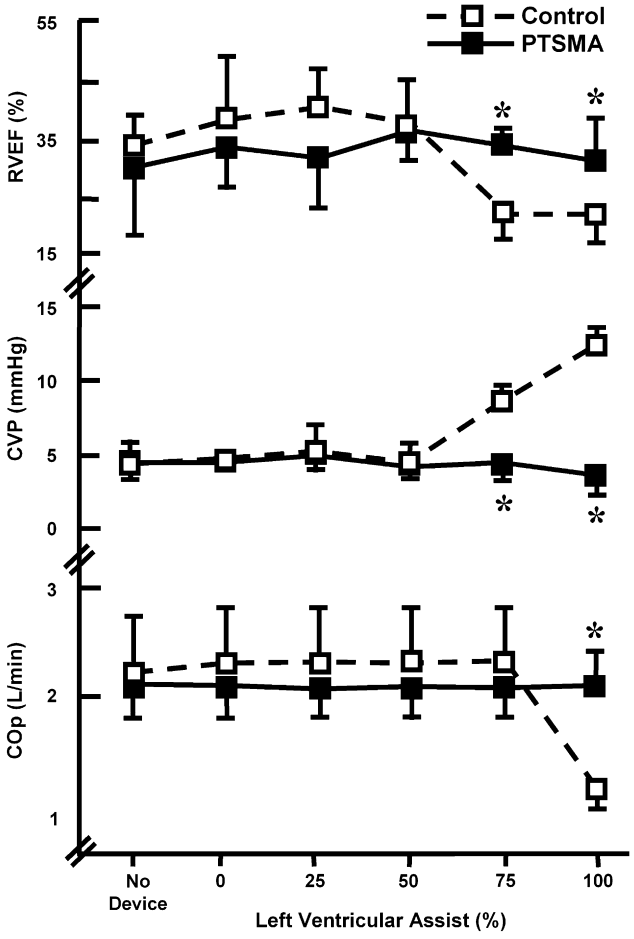

FIGURE 3. In-series hemodynamic effects of LV unloading in sham and PTSMA animals. *RVEF,* Right ventricular ejection fraction; *CVP,* central venous pressure; *COp,* pulmonary artery cardiac output; *PTSMA,* percutaneous transluminal septal myocardial ablation.

equivalent PTSMA values (34.4 ± 5.5 mm and 29.1 ± 5.5 mm vs 25.6 ± 4.7 mm and 20.5 ± 4.0 mm; $P \leq .01$). This pattern persisted with 100% unloading (37.6 ± 6.6 mm and 29.9 ± 5.9 mm vs 25.5 ± 3.9 mm and 21.1 ± 3.8 mm; $P \leq .01$).

Contrasting those of the RV, LV ED and ES internal short-axis dimensions decreased from 46.1 ± 4.4 mm with 50% to 37.7 ± 5.0 mm with 75% unloading in shams versus 41.7 ± 6.2 mm and 34.5 ± 2.5 mm in PTSMA ($P \leq 0.01$), and persisted with 100% unloading (40.1 ± 6.3 mm and 32.7 ± 2.6 mm in sham vs 46.3 ± 4.1 mm and 39.0 ± 3.9 mm in PTSMA; $P \leq .01$).

In PTSMA animals, internal ventricular dimensions were preserved across all levels of LV unloading and averaged 25.3 ± 3.9 and 20.3 ± 3.7 for ED and ES in the RV and 46.3 ± 4.5 and 38.8 ± 4.2 for ED and ES in the LV. Summative RV and LV dimensions remained unchanged for both sham and PTSMA animals.

Validation of Septal Dysfunction

Effects of PTSMA on regional septal, LV, and RV free wall thickening are summarized in Figure 4, *A,* which shows a reduction in septal thickening in PTSMA animals compared with sham (18.1% ± 2.6% vs 6.9% ± 3.6%; $P \leq .01$) and no difference between groups in free wall thickening (14.1% ± 3.7% and 4.5% ± 2.3% vs 13.7% ± 3.6% and 4.8% ± 3.5%, respectively). PTSMA animals had increased paced beats compared with sham (25.6% ± 11.1% vs 3.9% ± 2.7%, $P \leq .01$, Figure 4, *B*).

MSPA supply regions were similar in the 2 groups (sham vs PTSMA: 38.2% ± 5.3% and 38.3% ± 6.1% of the LV-septal surface area, $P = .956$; 40.2% ± 13.9% and 36.3% ± 9.2% of the RV-septal surface area, $P = .575$, 26.2.2% ± 10.8% and 25.8% ± 8.4% of total septal weight, $P = .962$). Histologic effects of PTSMA were confined to the septum (Figure 5), where necrotic tissue by triphenyltetrazolium perfusion in ablated septa was higher at 18.7% ± 2.0% of the septal tissue by weight compared with 4.7% ± 8.5% of sham ($P = .014$).

ET/BS

TABLE 1. LV, RV, and summed internal dimensions at end diastole and end systole in sham and PTSMA animals during increasing levels of LV unloading

	0		25		50		75		100	
LVAD unloading (%)	**ED**	**ES**	**ED**	**ES**	**ED**	**ES**	**ED**	**ES**	**ED**	**ES**
RV ID										
S	27.9 ± 6.6	22.3 ± 6.2	27.2 ± 5.9	22.5 ± 5.9	27.8 ± 6.0	21.7 ± 5.9	34.4 ± 5.5*	29.1 ± 5.5*	37.6 ± 6.6*	29.9 ± 5.9*
P	25.6 ± 4.4	20.9 ± 4.2	24.7 ± 3.7	19.8 ± 3.4	25.3 ± 4.1	19.4 ± 4.1	25.6 ± 4.7*	20.5 ± 4.0*	25.5 ± 3.9*	21.1 ± 3.8*
LV ID										
S	47.7 ± 3.2	39.6 ± 2.4	47.2 ± 3.2	39.2 ± 3.4	46.1 ± 4.4	37.7 ± 5.0	41.7 ± 6.2*	34.5 ± 2.5*	40.1 ± 6.3*	32.7 ± 2.6*
P	48.1 ± 5.0	40.3 ± 4.0	46.7 ± 4.6	39.3 ± 4.0	45.5 ± 4.9	38.2 ± 5.1	44.7 ± 4.8*	37.3 ± 5.9*	46.3 ± 4.1*	39.0 ± 3.9*
Summed ventricular ID										
S	75.6 ± 7.7	61.9 ± 6.9	74.4 ± 7.9	61.5 ± 7.8	73.9 ± 7.9	59.4 ± 7.9	76.1 ± 7.6	63.7 ± 5.2	77.7 ± 4.8	62.6 ± 6.4
P	73.7 ± 7.7	61.1 ± 7.3	71.4 ± 7.0	59.1 ± 6.7	70.7 ± 8.0	57.6 ± 7.7	70.4 ± 7.8	57.8 ± 7.0	71.9 ± 6.1	60.1 ± 6.7

LVAD, Left ventricular assist device; *RV*, right ventricle; *LV*, left ventricle; *ED*, end diastolic; *ES*, end systolic; *ID*, internal dimension; *S*, sham, *P*, PTSMA. * Statistical significance ($P \leq .01$) between sham and PTSMA groups.

DISCUSSION

The major findings of the present study are that 75% or greater LV unloading (i) induces LV volume reduction and RV volume expansion that contribute to load-independent RV dysfunction and (ii) leads to deterioration of in-series hemodynamic function, resulting in RV failure. Also, in the presence of chronic septal injury (iii) RV geometry and load-independent and in-series function are preserved, and (iv) this RV protection results from chronic septal fibrosis and associated septal dysfunction.

Load-Independent and Geometric Right Ventricular Response to Left Ventricular Unloading

It is clear from our results on load-independent and geometric findings that 75% or greater unloading degrades intrinsic load-independent RV function in normal hearts. This finding reinforces in-series hemodynamic changes at equivalent levels of unloading and is substantiated by geometric data. The two combine to cause collapse of the LV and dilatation of the RV. This finding supports the results of load-dependent investigations,[7] but contrasts with findings of load-independent function that suggests their preservation while in-series hemodynamic function deteriorates.[9] These differences may relate to the degree of unloading achieved and the more robust assessment of RV volume used in our experiments.[17] Summative ventricular dimensions were unaltered across all levels of unloading irrespective of septal damage, demonstrating that RV dilatation in sham animals is offset by LV collapse during high assist levels. As the first such study to demonstrate this, it extends previous findings limited to RV assessment that have confined observation to RV shape change, RV dilatation, and septal shift.[7,8,21] In support of studies suggesting septal position directly influences biventricular function, we have demonstrated that RV geometric disruption directly leads to altered RV function during high levels of LV unloading in normal hearts.

Geometric analysis identified 75% or greater LV unloading induces leftward septal shift, which appeared at a 75% threshold where it also reached a maximum. This state was maintained with 100% unloading, making it likely that the 36F cannula traversing the left atrium and mitral valve limited further septal movement. Conversely, mechanical devices using direct LV apical cannulation, such as the axial flow devices, may add a component of base-to-apical ''suction'' and induce even greater degrees of LV collapse with

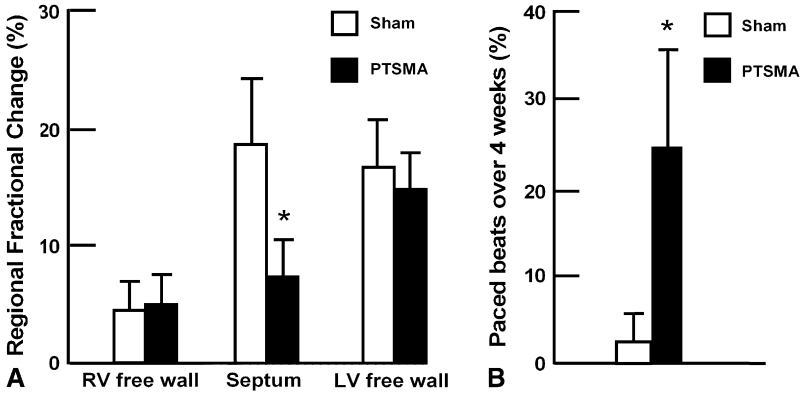

FIGURE 4. A, Chronic regional effects of PTSMA on interventricular septum and RV and LV free wall thickening. B, Effect of PTSMA on need for pacing. *RV*, Right ventricle; *LV*, left ventricle; *PTSMA*, percutaneous transluminal septal myocardial ablation.

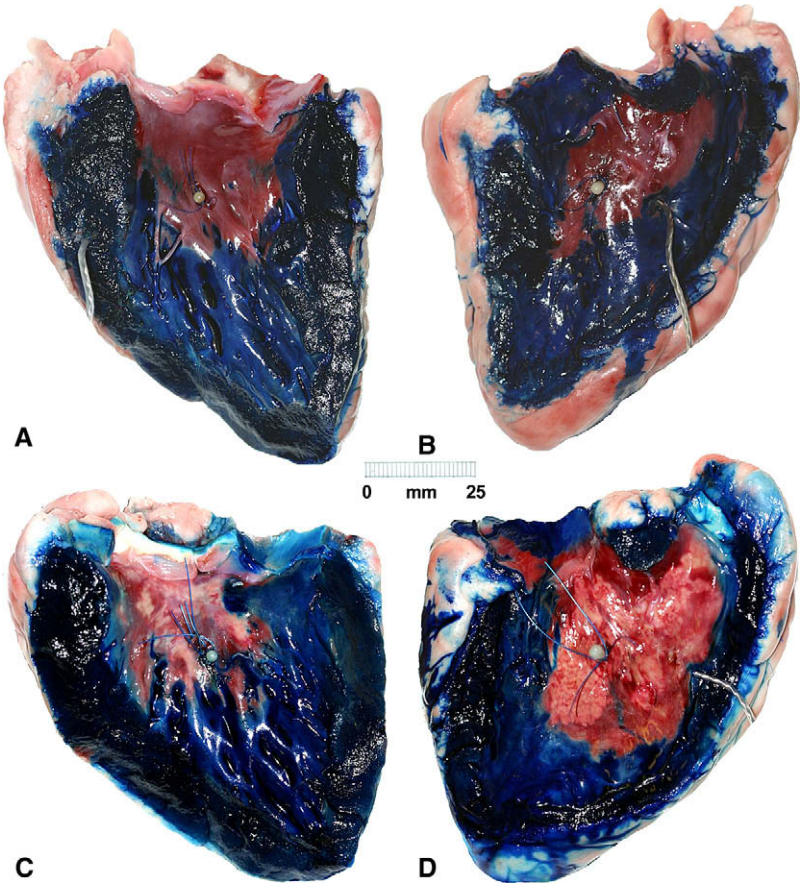

FIGURE 5. Sham (A, B) and PTSMA (C, D) postmortem hearts before removal of septal sonomicrometer crystals and after differential staining with 1% triphenyltetrazolium solution and methylene blue dye. Extensive fibrosis (*white*) is seen on the *left* (C) and *right* (D) septal surfaces after PTSMA, whereas undamaged triphenyltetrazolium stained *red* areas (A, B) are seen in the sham.

high assist levels. We have demonstrated that protection from RV dilatation is provided by the presence of chronic septal damage. This is the first study to identify clear differences in RV response to septal infarction compared with reversible ischemia. Despite previous investigation indicating that septal ischemia to be a primary etiological factor leading to RV failure during mechanical LV assistance,[13] we found that permanent septal injury in sheep hearts elicit an opposing effect. Coupled with preservation of RV geometry, it is likely that protection is due to impaired septal compliance resulting from PTSMA-induced fibrosis that limits movement into the LV cavity. Neurohormonal activation in infarcted animals may further influence this interaction.

Load-Dependent Right Ventricular Response to Left Ventricular Unloading

Increases in CVP, RV end-diastolic volume, and pulmonary wedge pressure during high levels of LV unloading have been assumed to result from increased venous return related to an increase from mechanically assisted CO.[22] Our results support these findings, evidenced by a decrease in RV EF and an increase in CVP, by suggesting that between 50% and 75% LV unloading, the redundancy of load-dependent RV function is curtailed. The persistent decrease in RV EF demonstrated at 75% or greater unloading also agrees with other studies examining septal position.[7,23]

Verification of Septal Dysfunction

In keeping with previous clinical studies that have examined the effect of PTSMA,[14,24] our findings show that PTSMA results in a significant chronic localized infarct after 4 weeks. Our moderate dose of ethanol maximized chronic damage while minimizing the potential complications, such as complete heart block and retrograde left anterior descending infarction. No animal in our series had such complications during hemodynamic assessment, but interrogation at 4 weeks of standby pacemakers identified an increased pacing need (Figure 4), indicative of temporary His-Bundle dysfunction resulting from edema.

Study Limitations

RV and LV function were assessed in an experimental model designed to address specific physiologic questions. Heterogeneity of such clinical disease as heart failure was

avoided to reduce the potential confounding effects. Further, we have not applied the septal injury model to a failing heart to mimic the clinical setting for use of LVADs. Such a study forms the basis of further investigation.

CONCLUSIONS

RV dysfunction after LV unloading has been traditionally attributed to enhanced venous return acting on occult RV pathology,[25] iatrogenic LV collapse, and RV dilatation with interruption of left and right coupling mechanisms.[7,8,12,21,23] We have identified the normal sheep heart as *more* susceptible to RV dysfunction during high levels of LV unloading compared with that with chronic septal injury. This confirms that the previous postulated etiological role of septal ischemia in RV dysfunction and intractable failure demonstrated in a large animal model[13] is not applicable to chronic septal pathologies. Thus, clinically, patients with significant septal fibrosis may be protected during LV cardiac assistance from the greater risk of RV dysfunction that is an accompaniment of ''normal'' or ischemic interventricular septa.

Compared with the results of previous studies of acute ischemic septal dysfunction, these studies demonstrate a distinctly different RV response during high levels of LV unloading with chronic septal pathology. This warrants more investigation into the clinical manifestation of refractory RV failure during LV unloading, especially in patients who demonstrate evidence of chronic dysfunction and require mechanical CO augmentation.

We thank Dr Henning Bundgaard for assistance with catheterization procedures; Bruce Williams, the late Ray Kearns, Wayne Roach, Cathy Mundy, and Kellie Tinworth for technical assistance; and Medtronic Inc, which via Chris McLure, supplied and advised on use of pacemakers. Daryl McMillan as perfusionist, gave valuable assistance and advice on LV unloading.

ET/BS

References

1. Lietz K, Long JW, Kfoury AG, Slaughter MS, Silver MA, Milano CA, et al. Outcomes of left ventricular assist device implantation as destination therapy in the post-REMATCH era: implications for patient selection. *Circulation*. 2007;116:497-505.
2. Drakos SG, Charitos EI, Nanas SN, Nanas JN. Ventricular-assist devices for the treatment of chronic heart failure. *Expert Rev Cardiovasc Ther*. 2007;5:571-84.
3. Stone ME. Current status of mechanical circulatory assistance. *Semin Cardiothorac Vasc Anesth*. 2007;11:185-204.
4. Dang NC, Topkara VK, Mercando M, Kay J, Kruger KH, Aboodi MS, et al. Right heart failure after left ventricular assist device implantation in patients with chronic congestive heart failure. *J Heart Lung Transplant*. 2006;25:1-6.
5. Furukawa K, Motomura T, Nose Y. Right ventricular failure after left ventricular assist device implantation: the need for an implantable right ventricular assist device. *Artif Organs*. 2005;29:369-77.
6. Morgan JA, John R, Lee BJ, Oz MC, Naka Y. Is severe right ventricular failure in left ventricular assist device recipients a risk factor for unsuccessful bridging to transplant and post-transplant mortality. *Ann Thorac Surg*. 2004;77:859-63.
7. Moon MR, Castro LJ, DeAnda A, Tomizawa Y, Daughters GT 2nd, Ingels NB Jr, et al. Right ventricular dynamics during left ventricular assistance in closed-chest dogs. *Ann Thorac Surg*. 1993;56:54-67.
8. Morita S, Kormos RL, Mandarino WA, Eishi K, Kawai A, Gasior TA, et al. Right ventricular/arterial coupling in the patient with left ventricular assistance. *Circulation*. 1992;86:II316-25.
9. Elbeery JR, Owen CH, Savitt MA, Davis JW, Feneley MP, Rankin JS, et al. Effects of the left ventricular assist device on right ventricular function. *J Thorac Cardiovasc Surg*. 1990;99:809-16.
10. Buckberg GD. The ventricular septum: the lion of right ventricular function, and its impact on right ventricular restoration. *Eur J Cardiothorac Surg*. 2006;29:S272-8.
11. Saleh S, Liakopoulos OJ, Buckberg GD. The septal motor of biventricular function. *Eur J Cardiothorac Surg*. 2006;29:S126-38.
12. Klima UP, Lee MY, Guerrero JL, Laraia PJ, Levine RA, Vlahakes GJ. Determinants of maximal right ventricular function: role of septal shift. *J Thorac Cardiovasc Surg*. 2002;123:72-80.
13. Daly RC, Chandrasekaran K, Cavarocchi NC, Tajik AJ, Schaff HV. Ischemia of the interventricular septum. A mechanism of right ventricular failure during mechanical left ventricular assist. *J Thorac Cardiovasc Surg*. 1992;103:1186-91.
14. Veselka J, Duchonova R, Prochazkova S, Palenickova J, Sorajja P, Tesar D. Effects of varying ethanol dosing in percutaneous septal ablation for obstructive hypertrophic cardiomyopathy on early hemodynamic changes. *Am J Cardiol*. 2005;95:675-8.
15. Veselka J, Prochazkova S, Duchonova R, Bolomova-Homolova I, Palenickova J, Tesar D, et al. Alcohol septal ablation for hypertrophic obstructive cardiomyopathy: lower alcohol dose reduces size of infarction and has comparable hemodynamic and clinical outcome. *Catheter Cardiovasc Interv*. 2004;63:231-5.
16. Van Dockum WG, Ten Cate FJ, Ten Berg JM, Beek AM, Twisk JWR, Vos J, et al. Myocardial infarction after percutaneous transluminal septal myocardial ablation in hypertrophic obstructive cardiomyopathy: Evaluation by contrast-enhanced magnetic resonance imaging. *J Am Coll Cardiol*. 2004;43:27-34.
17. Mau JC, Menzie SJ, Ward MR, Bundgaard H, Hunyor SN. Time-dependent response of both ventricles after septal ablation: implications for biventricular support after left ventricular assist device placement. *J Thorac Cardiovasc Surg*. 2007;134:579-86.
18. McConnell PI, Del Rio CL, Kwiatkowski P, Farrar DJ, Sun BC. Assessment of cardiac function during axial-flow left ventricular assist device support using a left ventricular pressure-derived relationship: comparison with pre-load recruitable stroke work. *J Heart Lung Transplant*. 2007;26:159-66.
19. Feneley MP, Elbeery JR, Gaynor JW, Gall SAJ, Davis JW, Rankin JS. Ellipsoidal shell subtraction model of right ventricular volume: comparison with regional free wall dimensions as indexes of right ventricular function. *Circ Res*. 1990;67:1427-36.
20. Ramanathan T, Shirota K, Morita S, Nishimura T, Huang Y, Hunyor SN. Glucose-insulin-potassium solution improves left ventricular mechanics in diabetes. *Ann Thorac Surg*. 2002;73:582-7.
21. Moon MR, Bolger AF, DeAnda A, Komeda M, Daughters GT, Nikolic SD, et al. Septal function during left ventricular unloading. *Circulation*. 1997;95:1320-7.
22. Farrar DJ, Chow E, Wood J, Hill JD. Comparison of right ventricular and biventricular circulatory support in a porcine model of right heart failure. *ASAIO Trans*. 1990;36:M522-5.
23. Mandarino WA, Morita S, Kormos RL, Kawai A, Deneault LG, Gasior TA, et al. Quantitation of right ventricular shape changes after left ventricular assist device implantation. *ASAIO J*. 1992;38:M228-31.
24. Burri H, Sigwart U. Technology insight: transcoronary ablation of septal hypertrophy. *Nat Clin Pract Cardiovasc Med*. 2005;2:101-7.
25. Goldstein JA. Pathophysiology and clinical management of right heart ischemia. *Curr Opin Cardiol*. 1999;14:329-39.